

## ARTICLE TEMPLATE

### **Automated assessment of residual plots with computer vision models**

Weihao Li<sup>a</sup>

<sup>a</sup>Department of Econometrics and Business Statistics, Monash University, Clayton, VIC,  
Australia

#### **ARTICLE HISTORY**

Compiled February 6, 2024

#### **ABSTRACT**

TBD.

#### **KEYWORDS**

TBD

## Contents

<b>1</b>	<b>Introduction</b>	<b>4</b>
<b>2</b>	<b>Methodology</b>	<b>7</b>
2.1	Different possible configurations of the model formula . . . . .	7
2.1.1	Different input formats . . . . .	7
2.1.2	Different output formats . . . . .	9
2.2	Distance from the good residual plots . . . . .	9
2.2.1	Residual distribution . . . . .	10
2.2.2	Kullback-Leibler divergence of $P$ from $Q$ . . . . .	11
2.2.3	Evaluation of Kullback-Leibler divergence for non-normal $P$ . .	12
2.2.4	Approximation of the distance metric . . . . .	13
2.3	Statistical testing based on the approximated distance . . . . .	14
2.3.1	Null distribution of the approximated distance . . . . .	14
2.3.2	Estimation of quantiles of the null distribution . . . . .	15
2.3.3	Bootstrapping the approximated distance . . . . .	16
2.4	Generation of training data . . . . .	17
2.4.1	Data generating process . . . . .	17
2.4.2	Computation of scagnostics . . . . .	18
2.4.3	Crafting a balanced training set . . . . .	19
2.5	Architecture of the computer vision model . . . . .	19
2.6	Training and hyperparameter tuning . . . . .	21
2.7	Model evaluation methods . . . . .	22
<b>3</b>	<b>Results</b>	<b>23</b>
3.1	Optimized hyperparameters . . . . .	23
3.2	Model performance . . . . .	24
3.3	Comparison with human visual inference . . . . .	24
3.3.1	Overview of the human subject experiment . . . . .	24
3.3.2	Model performance on the human data . . . . .	26
3.4	When the model works . . . . .	29

3.5	When the model does not work . . . . .	29
3.6	Workflow: how one use this model? (small showcase) . . . . .	34
<b>4</b>	<b>Dicussion</b>	<b>34</b>
<b>5</b>	<b>Conclusion</b>	<b>34</b>

## 1. Introduction

Plotting residuals is commonly regarded as a standard practice in linear regression diagnostics (see Cook and Weisberg 1982; Belsley, Kuh, and Welsch 1980). This visual assessment plays a crucial role in identifying deviations from model assumptions, such as linearity, homoscedasticity, and normality. It also helps in understanding the goodness of fit and various characteristics of the model.

Generating a residual plot in most statistical software is often as straightforward as executing a line of code or clicking a button. However, accurately interpreting a residual plot can be challenging. Consider Figure 1 as an example, the residuals display a triangular shape pointing to the left. While this might suggest heteroskedasticity, it is important to avoid over-interpreting this visual pattern. In this case, the fitted model is correctly specified, and the triangular shape is actually a result of the skewed distribution of the predictors, rather than indicating a flaw in the model.

A residual plot can exhibit various visual features, but it is crucial to recognize that some may arise from the characteristics of predictors and the inherent randomness of the error, rather than indicating a violation of model assumptions (Li et al. 2023). The concept of visual inference, as proposed by Buja et al. (2009), provides an inferential framework to assess whether residual plots indeed contain visual patterns inconsistent with the model assumptions. The fundamental idea involves testing whether the actual residual plot visually differs significantly from null plots, which are created using residuals generated from the null distribution. Typically, this is accomplished through the lineup protocol. In this approach, the real residual plot is embedded within a lineup alongside several null plots. If the real residual plot can be distinguished from the lineup, it provides evidence for rejecting the null hypothesis.

The practice of delivering a residual plot as a lineup is generally regarded as a valuable approach. Beyond its application in residual diagnostics, the lineup protocol has integrated into the analysis of diverse subjects. For instance, Loy and Hofmann (2013, 2014, 2015) illustrate its applicability in diagnosing hierarchical linear models. Additionally, Widen et al. (2016) demonstrates its utility in geographical research, while Krishnan and Hofmann (2021) explores its effectiveness in forensic examinations.

However, as pointed out by Li et al. (2023), a primary limitation of the lineup protocol lies in its reliance on human judgments. Unlike conventional statistical tests that can be performed computationally in statistical software, the lineup protocol requires human evaluation of images. This characteristic makes it less suitable for large-scale applications, given the associated high labor costs and time requirements.

There is a substantial need to develop an approach that alleviates analysts’ workload by automating repetitive tasks and providing standardized results in a controlled environment. The large-scale evaluation of lineups is impractical without the use of technology and machines.

The utilization of computers to interpret data plots has a rich history, with early efforts such as “Scagnostics” by Tukey and Tukey (1985), focusing on scatterplot diagnostics. Wilkinson, Anand, and Grossman (2005) expanded on this work, introducing graph theoretic scagnostics, which encompassed nine computable measures applied to planar proximity graphs. These measures, including, but not limited to, “Outlying”, “Skinny”, “Stringy”, “Straight”, “Monotonic”, “Skewed”, “Clumpy”, and “Striated” aimed to characterize outliers, shape, density, trend, coherence and other characteristics of the data. While this approach has been inspiring, there is a recognition (Buja et al. 2009) that it may not capture all the necessary visual features that differentiate actual residual plots from null plots. A more promising alternative entails enabling computers to learn the function for extracting visual features from residual plots. Essentially, this means empowering computers to discern the crucial visual features for residual diagnostics and determining the method to extract them. Modern computer vision models are well-suited for addressing this challenge.

Modern computer vision models often rely on deep neural networks with convolutional layers (Fukushima and Miyake 1982). These layers leverage hierarchical patterns in data, downsizing and transforming images by summarizing information in a small space. Numerous studies have demonstrated the efficacy of convolutional layers in addressing various vision tasks, including image recognition (Rawat and Wang 2017). Despite the widespread use of computer vision models in fields like computer-aided diagnosis (Lee and Chen 2015), pedestrian detection (Brunetti et al. 2018), and facial recognition (Emami and Suci 2012), their application in reading data plots remains

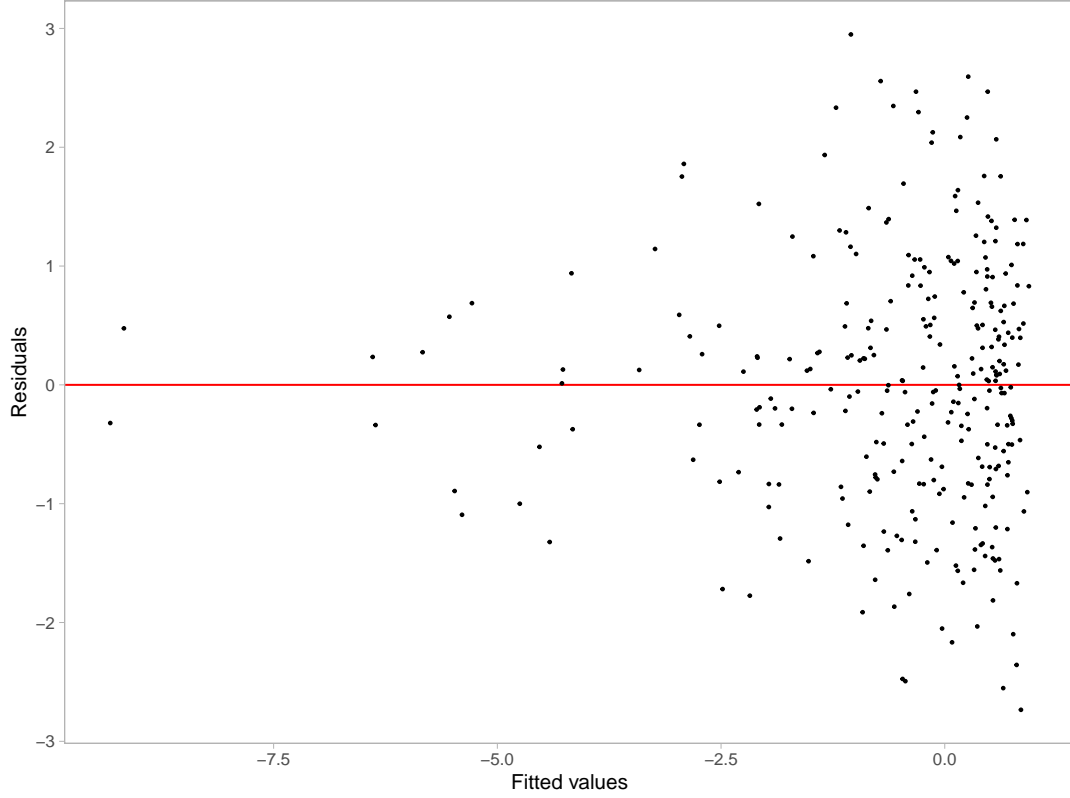


**Figure 1.** An example residual vs fitted values plot (red line indicates 0). The vertical spread of the data points varies with the fitted values. This often indicates the existence of heteroskedasticity.

limited. While some studies have explored the use of computer vision models for tasks such as reading recurrence plots for time series regression (Ojeda, Solano, and Peramo 2020), time series classification (Chu et al. 2019; Hailesilassie 2019; Hatami, Gavet, and Debayle 2018; Zhang et al. 2020), anomaly detection (Chen, Su, and Yang 2020), and pairwise causality analysis (Singh et al. 2017), the application of reading residual plots with computer vision models represents a relatively new field of study.

In this paper, we develop computer vision models and integrate them into the residual plots diagnostics workflow, filling the gap of. . . The paper is structured as follows: . . .

## 2. Methodology

### 2.1. *Different possible configurations of the model formula*

There are various configurations of the computer vision model that can be used to assess residual plots. We discuss these configurations below based on two key components of the model formula: the input and the output format.

#### 2.1.1. *Different input formats*

Deep learning models are in general very sensitive to the input data. The quality and relevance of the input data greatly influence the model’s capacity to generate insightful and meaningful results.

A straightforward approach involves feeding a vector of residuals along with a vector of fitted values, essentially providing all the necessary information for creating a residuals vs fitted values plot. However, a drawback of this method is the dynamic input size, which changes based on the number of observations. For modern computer vision models implemented in mainstream software like TensorFlow (Abadi et al. 2016), the input shape is typically fixed. One solution is to pad the input vectors with leading or trailing zeros when the input tensor expects longer vectors, but it may fail if the input vector surpasses the designed length. Another strategy is to summarize the residuals and fitted values separately using histograms and utilize the counts as the input. By controlling the number of bins in the histograms, it becomes possible to provide fixed-length input vectors. Still, since the histogram only captures the marginal distribution of residuals and fitted values respectively, it can not be used to differentiate visual patterns with same marginal distributions but different joint distributions.

Another approach is to use an image as input. The primary advantage of using an image, as opposed to the vector format, is the utilization of the sophisticated image processing architectures developed over the years, such as the VGG16 architecture proposed in Simonyan and Zisserman (2014). These architectures can effectively capture and summarize spatial information from nearby pixels, which is less straightforward with vector input. The only considerations are the image resolution and the aesthetics of the residual plot. In general, higher resolution provides more information to the

model but comes with the trade-off of increased complexity and greater difficulty in training. As for the aesthetics of the residual plot, a practical solution is to consistently present residual plots in the same style to the model. This implies that the model can not accept arbitrary images as input but requires the use of the same preprocessing software to convert provided residuals and fitted values into a standardized style for the residual plot.

Providing multiple residual plots to the model, such as a pair of plots, a triplet or a lineup is also a possible option. Chopra, Hadsell, and LeCun (2005) has shown that computer vision models designed for image comparison can assess whether a pair of images are similar or dissimilar. Applied to our specific problem, we can define null plots of a fitted model to be similar to each other, while considering actual residual plots to be distinct from null plots of any fitted model. A triplet constitutes a set of three images, denoted as  $image_1$ ,  $image_2$  and  $image_3$ . It is often used to predict whether  $image_2$  or  $image_3$  is more similar to  $image_1$ , proving particularly useful for establishing rankings between samples. For this setup, we can apply the same criteria to define similarity between images. However, it’s important to note that these two approaches usually require additional considerations regarding the loss function and, at times, non-standard training processes due to shared weights between different convolutional blocks.

Presenting a lineup to a model and asking it to predict which residual plot is the most different one aligns closely with the lineup protocol. However, if a lineup consists of a large amount of residual plots, the resolution of the input image could become quite large, posing challenges in training the model. This approach was experimented in a pilot study conducted by us but the performance of the trained model was sub-optimal.

We did not explore all the mentioned input formats due the considerable costs associated with data preparation and model training. Considering the implementation cost and the interpretability of the model, we settled on the single residual plot input format.



### *2.1.2. Different output formats*

Given that the input is a single residual plot represented as a fixed-resolution image, the output from the computer vision model can take one of two formats: binary or numeric. This choice determines whether the model belongs to a classification model or a regression model. The binary outcome could be designed to indicate whether the input image is a null plot, or whether the input image would be rejected in a visual test conducted by humans. The latter option requires data from prior human subject experiments, presenting difficulties in controlling the quality of data due to variations in experimental settings across different studies. Additionally, some visual inference experiments are unrelated to linear regression models and residual plot diagnostics, resulting in a limited amount of available training data.

Alternatively, the output could be designed as a meaningful numeric measure, such as the average distance to good residual plots. This approach necessitates defining a distance measure between residual plots, which may be a non-trivial task. However, once a meaningful distance measure is established, the prediction from the computer vision model becomes an interpretable value with tangible significance. Studies have demonstrated that defining a proper distance between images can enhance the matching accuracy in image search compared to a binary outcome model (ref here).

## ***2.2. Distance from the good residual plots***

In a visual test, the observer will be asked to choose one or more plots that stand out as most distinct from others in a given lineup. To develop a computer vision model for assessing residual plots within the visual inference framework, it is important to precisely define a numerical measure of “difference” or “distance” between plots. This distance can take the form of a basic statistical operation on pixels, such as the sum of square differences. Alternatively, it could involve established image similarity metrics like the Structural Similarity Index Measure (Wang et al. 2004). The challenge lies in the fact that metrics tailored for image comparison may not be suitable for evaluating data plots, where only essential plot elements require assessment (Chowdhury et al. 2018). Furthermore, scagnostics mentioned in Section 1 could be used to construct

distance metrics for data plots comparison, but the functional form still needs to be carefully refined to accurately reflect the extent of the violations.

### 2.2.1. Residual distribution

The distance metrics proposed in this paper takes into account the fact that we try to measure how different a residual plot is from a good residual plot, or in other words, how different a given fitted model is from a correctly specified model. For the classical normal linear regression model, residuals  $\mathbf{e}$  are derived from the fitted values  $\hat{\mathbf{y}}$  and observed values  $\mathbf{y}$ . Suppose the data generating process is known and the regression model is correctly specified, by the Frisch-Waugh-Lowell theorem (Frisch and Waugh 1933), residuals  $\mathbf{e}$  can also be treated as random variables and written as a linear transformation of the error  $\boldsymbol{\varepsilon}$  formulated as  $\mathbf{e} = \mathbf{R}\boldsymbol{\varepsilon}$ , where  $\mathbf{R} = \mathbf{I}_n - \mathbf{X}(\mathbf{X}'\mathbf{X})^{-1}\mathbf{X}'$  is the residual operator and an idempotent matrix,  $\mathbf{X}$  is the design matrix,  $\mathbf{I}_n$  is a  $n$  by  $n$  identity matrix, and  $n$  is the number of observations.

One of the assumptions of the classical normal linear regression model is the error  $\boldsymbol{\varepsilon}$  follows a multivariate normal distribution with zero mean and constant variance, i.e.,  $\boldsymbol{\varepsilon} \sim N(\mathbf{0}_n, \sigma^2 \mathbf{I}_n)$ . It can be known that residuals  $\mathbf{e}$  also follow a certain probability distribution transformed from the multivariate normal distribution, which will be denoted as  $Q$ . This reference distribution  $Q$  summarizes what good residuals should follow given the predictors are known and fixed.

In ordinary least square, the minimization of the sum of square residuals implies  $\sum_{i=1}^n e_i = 0$ , making any residual value to be a linear combination of the remaining  $n - 1$  residuals. This effectively means  $\text{rank}(\mathbf{R}) = n - 1 < n$  and  $Q$  is a degenerate multivariate distribution. To capture the characteristics of  $Q$ , such as moments, we can simulate a large numbers of  $\boldsymbol{\varepsilon}$  and transform it to  $\mathbf{e}$  to get the empirical estimates. For simplicity, we replaced the variance-covariance matrix of residuals  $\text{cov}(\mathbf{e}, \mathbf{e}) = \mathbf{R}\sigma^2\mathbf{R}' = \mathbf{R}\sigma^2$  with a full-rank diagonal matrix  $\text{diag}(\mathbf{R}\sigma^2)$ , where  $\text{diag}(\cdot)$  sets the non-diagonal entries of a matrix to zeros. The resulting distribution for  $\mathbf{Q}$  is  $N(\mathbf{0}_n, \text{diag}(\mathbf{R}\sigma^2))$ .

Distribution  $Q$  is derived from the correctly specified model. However, if the model is misspecified, then the actual distribution of residuals denoted as  $P$ , will be different

from  $Q$ . For example, if the data generating process contains variables correlated with any column of  $\mathbf{X}$  but not included in  $\mathbf{X}$ , causing an omitted variable problem,  $P$  will be different from  $Q$  because the residual operator obtained from the fitted model will not be the same as  $\mathbf{R}$ . Besides, if the  $\boldsymbol{\varepsilon}$  follows a non-normal distribution such as a multivariate lognormal distribution,  $P$  will usually be skewed and has a long tail.

### 2.2.2. Kullback-Leibler divergence of $P$ from $Q$

Define a proper distance between distributions is usually easier than define a proper distance between data plots. Given the actual residual distribution  $Q$  and the reference residual distribution  $P$ , we used a distance metric based on Kullback-Leibler divergence (Kullback and Leibler 1951) to quantify the difference between two distributions

$$D = \log(1 + D_{KL}), \quad (1)$$

$$D_{KL} = \int_{\mathbb{R}^n} \log \frac{p(\mathbf{e})}{q(\mathbf{e})} p(\mathbf{e}) d\mathbf{e}, \quad (2)$$

where  $p(\cdot)$  is the probability density function for distribution  $P$ , and  $q(\cdot)$  is the probability density function for distribution  $Q$ .

This distance metric was first proposed in Li et al. (2023). It was mainly designed for measuring the effect size of non-linearity and heteroskedasticity in a residual plot. Li et al. (2023) showed that, for a classical normal linear regression model that omits a necessary higher-order predictors  $\mathbf{Z}$ , and incorrectly assumes  $\boldsymbol{\varepsilon} \sim N(\mathbf{0}_n, \sigma^2 \mathbf{I}_n)$  while in fact  $\boldsymbol{\varepsilon} \sim N(\mathbf{0}_n, \mathbf{V})$  with  $\mathbf{V}$  being an arbitrary symmetric positive semi-definite matrix,  $Q$  can be represented as  $N(\mathbf{RZ}\boldsymbol{\beta}_z, \text{diag}(\mathbf{RV}\mathbf{R}))$ . Note that the variance-covariance matrix is replaced with the diagonal matrix to ensure it is a full-rank matrix.

Since both  $P$  and  $Q$  are adjusted to be multivariate normal distributions, equation 2 can be further expanded to

$$D_{KL} = \frac{1}{2} \left( \log \frac{|\text{diag}(\mathbf{W})|}{|\text{diag}(\mathbf{R}\sigma^2)|} - n + \text{tr}(\text{diag}(\mathbf{W})^{-1} \text{diag}(\mathbf{R}\sigma^2)) + \boldsymbol{\mu}'_z (\text{diag}(\mathbf{W}))^{-1} \boldsymbol{\mu}_z \right), \quad (3)$$

where  $\boldsymbol{\mu}_z = \mathbf{RZ}\boldsymbol{\beta}_z$ , and  $\mathbf{W} = \mathbf{RVR}$ . The assumed error variance  $\sigma^2$  is set to be  $\text{tr}(\mathbf{V})/n$ , which is the expectation of the estimated variance.

### 2.2.3. Evaluation of Kullback-Leibler divergence for non-normal $P$

For non-normal error  $\boldsymbol{\varepsilon}$ , the actual residual distribution  $P$  is unlikely to be a multivariate normal distribution. Thus, equation 3 given in Li et al. (2023) will not be applicable to models with non-normality violations.

To evaluate the Kullback-Leibler divergence of non-normal  $P$  from  $Q$ , the fallback is to solve equation 2 numerically. However, since  $\mathbf{e}$  is a linear transformation of non-normal random variables, it is very common that the general form of  $P$  is unknown, meaning that we can not easily compute  $p(\mathbf{e})$  using a well-known probability density function. Additionally, even if  $p(\mathbf{e})$  can be calculated for any  $\mathbf{e} \in \mathbb{R}^n$ , it will be very difficult to do numerical integration over the  $n$  dimensional space, because  $n$  could be potentially very large.

In order to approximate  $D_{KL}$  in a practically computable manner, the elements of  $\mathbf{e}$  are assumed to be independent of each other. This assumption solves both of the issues mentioned above. First, we no longer need to integrate over  $n$  random variables. The result of equation 2 is now the sum of the Kullback-Leibler divergence evaluated for each individual residual thanks for the independence assumption. Second, it is not required to know the joint probability density  $p(\mathbf{e})$  any more. Instead, the evaluation of Kullback-Leibler divergence for an individual residual relies on the knowledge of the marginal density  $p_i(e_i)$ , where  $e_i$  is the  $i$ -th residual for  $i = 1, \dots, n$ . This is much easier to approximate through simulation. It is also worth mentioning that this independence assumption generally will not hold, since  $\text{cov}(e_i, e_j) \neq 0$  if  $\mathbf{R}_{ij} \neq 0$  for any  $1 \leq i < j \leq n$ , but its existence is essential for reducing the computational cost.

The algorithm for approximating equation 2 starts from simulating  $m$  sets of  $\boldsymbol{\varepsilon}$

according to the error distribution. The simulated errors are stored in a matrix  $\mathbf{A}$  with  $n$  rows and  $m$  columns, where each column of  $\mathbf{A}$  is a set of realized values of  $\boldsymbol{\varepsilon}$ . Then, we can get  $m$  sets of realized values of  $\boldsymbol{e}$  stored in the matrix  $\mathbf{B}$  by applying the residual operator  $\mathbf{B} = \mathbf{R}\mathbf{A}$ . Furthermore, kernel density estimation (KDE) with Gaussian kernel and optimal bandwidth selected by the Silverman's rule of thumb (Silverman 2018) is applied on each row of  $\mathbf{B}$  to estimate  $p_i(e_i)$  for  $i = 1, \dots, n$ . The KDE computation is done by the `density` function in R.

Since the Kullback-Leibler divergence can be viewed as the expectation of the log-likelihood ratio between distribution  $P$  and distribution  $Q$  evaluated on distribution  $P$ , we can reuse the simulated residuals in matrix  $\mathbf{B}$  to estimate the expectation by the sample mean. With the independence assumption, for non-normal  $P$ ,  $D_{KL}$  can be approximated by

$$D_{KL} \approx \sum_{i=1}^n \hat{D}_{KL}^{(i)}, \quad (4)$$

$$\hat{D}_{KL}^{(i)} = \frac{1}{m} \sum_{j=1}^m \log \frac{\hat{p}_i(B_{ij})}{q(B_{ij})}, \quad (5)$$

where  $\hat{D}_{KL}^{(i)}$  is the estimator of the Kullback-Leibler divergence for an individual residual  $e_i$ ,  $B_{ij}$  is the  $i$ -th row and  $j$ -th column entry of the matrix  $\mathbf{B}$ ,  $\hat{p}_i(\cdot)$  is the kernel density estimator of  $p_i(\cdot)$ ,  $q(\cdot)$  is the normal density function with mean zero and an assumed variance estimated as  $\widehat{\sigma^2} = \sum_{b \in \text{vec}(\mathbf{B})} (b - \sum_{b \in \text{vec}(\mathbf{B})} b/nm)^2 / (nm - 1)$ , and  $\text{vec}(\cdot)$  is the vectorization operator which turns a  $n \times m$  matrix into a  $nm \times 1$  column vector by stacking the columns of the matrix on top of each other.

#### 2.2.4. Approximation of the distance metric

In the previous sections, we have defined a distance metric given in equation 1 for quantifying the difference between the actual residual distribution  $P$  and an ideal reference distribution  $Q$ . You may have noticed that this distance metric can only be computed when the data generating process is known. In reality, we often have no knowledge about the data generating process, otherwise we do not need to fit a linear

regression model in the first place.

What we proposed in this paper is a method to approximate this distance with a residual plot. Let  $D$  be the result of equation 1 indicating the extent of the model violations, and our estimator  $\hat{D}$  is formulated as

$$\hat{D} = f_{CV}(V_{h \times w}(\mathbf{e}, \hat{\mathbf{y}})), \quad (6)$$

where  $V_{h \times w}(\cdot)$  is a plotting function that saves a residuals vs fitted values plot with fixed aesthetic as an image with  $h \times w$  pixels and three colour channels,  $f_{CV}(\cdot)$  is a computer vision model which takes an  $h \times w$  image as input and predicts the distance in the domain  $[0, +\infty)$ .

With the approximated distance  $\hat{D}$ , we will be able to know how different the underlying distribution of the residuals is from a good residual distribution. This is meaningful way to check if a residual plot is a good residual plot, and to know the strength of the visual signal embedded in the residual plot.

The approximated distance  $\hat{D}$  is not expected to be the same as the original distance  $D$ . This is largely because information contained in a single residual plot is limited and it may not be able to summarise all the characteristics of the residual distribution. For a given residual distribution  $P$ , we can generate many different residual plots. Some of them share similar visual patterns, but some of them could be visually very different from the rest, especially for models with small  $n$ . This suggests the error of the approximation will vary depends on whether the observed residual plot is representative or not.

### **2.3. Statistical testing based on the approximated distance**

#### *2.3.1. Null distribution of the approximated distance*

Theoretically, the distance  $D$  for a correctly specified model is 0, because  $P$  will be the same as  $Q$ . However, the computer vision model may not necessary predict 0 for a null plot. Using Figure 1 as an example, it contains a visual pattern which is

an indication of heteroskedasticity. We would not expect the model to be able to magically tell if the suspicious pattern is caused by the skewed distribution of the fitted values or the existence of heteroskedasticity. Additionally, some null plots could have outliers or strong visual patterns due to randomness, and a reasonable model will try to summarise those information into the prediction, resulting in  $\hat{D} > 0$ .

This property is not an issue if  $\hat{D} \gg 0$  for which the visual signal of the residual plot is very strong, and we usually do not need any further examination of the significance of the result. However, if the visual pattern is weak or moderate, having  $\hat{D}$  will not be sufficient to determine if  $H_0$  that the model is correctly specified should be rejected.

To solve this issue while aligning with the principle of visual inference, the approximated distance  $\hat{D}$  can be viewed as a test statistic. And the null distribution of this statistic can be approximated by the empirical distribution of  $\hat{D}_{null}$  for a large amount of null plots of a fitted model. The procedure involves applying the residual rotation technique (Buja et al. 2009) on the fitted model to obtain null residuals. The null residuals are then used to make null plots and fed into the model to get predictions. The empirical distribution is constructed with the predicted distance.

There are two types of error associated with the approximation of the null distribution. These include the sampling error and the estimation error for model parameters. Increasing the number of null plots within the distribution approximation can effectively reduce sampling error. However, the estimation error for model parameters remains irreducible. The residual rotation technique operates under the assumption of a correct fitted model, using the estimated variance instead of the unknown true variance to rescale rotated residuals. Consequently, under  $H_0$ , the true distribution of  $\hat{D}_{null}$  will slightly deviate from the approximated null distribution.

### 2.3.2. Estimation of quantiles of the null distribution

Let  $\hat{D}_{null}^{(i)}$  be the predicted distance of the  $i$ -th null plots, where  $i = 1, \dots, n_{null}$  and  $n_{null} \in \mathbb{N}^+$  is a sufficiently large number. Quantiles of the null distribution can then be estimated using the sample quantiles available in statistical software such as R. The details of the sample quantile computation can be found in Hyndman and Fan (1996). In statistical testing, analysts often care about certain quantiles of the null distribution,

such as the 90% quantile, the 95% quantile and the 99% quantile. These quantiles are used as thresholds to decide if  $H_0$  needs to be rejected. For example, if  $\hat{D}$  is greater than and equal to the 95% sample quantile of the null distribution  $Q_{null}(0.95)$ , we could say the predicted distance for the actual residual plot is significantly different from the predicted distance for null plots with 95% significance level. Based on our experience, in order to get a stable estimate of the 95% quantile,  $n_{null}$  usually needs to be at least 100. And if the null distribution has a long tail, more null plots will be needed. Alternatively, a p-value can be used to represent the probability of observing an event equally or more extreme than the given event under  $H_0$ , and it can be estimated by  $1/m \sum_{i=1}^{n_{null}} I(\hat{D}_{null}^{(i)} \geq \hat{D})$ .

### 2.3.3. Bootstrapping the approximated distance

Bootstrap is often employed in linear regression when conducting inference for estimated parameters. It is typically done by sampling individual cases with replacement and refitting the regression model. If the observed data accurately reflects the true distribution of the population, the bootstrapped estimates can be used to measure the variability of the parameter estimate without making strong distributional assumptions about the data generating process.

Similarly, bootstrap can be applied on the approximated distance  $\hat{D}$ . For each refitted model  $M_{boot}^{(i)}$ , there will be an associated residual plot  $V_{boot}^{(i)}$  which can be fed into the computer vision model to obtain  $\hat{D}_{boot}^{(i)}$ , where  $i = 1, \dots, n_{boot}$ , and  $n_{boot}$  is the number of bootstrapped samples. If we are interested in the variation of  $\hat{D}$ , we can use  $\hat{D}_{boot}^{(i)}$  to estimate a confidence interval.

Alternatively, since each  $M_{boot}^{(i)}$  has a set of estimated coefficients  $\hat{\beta}_{boot}^{(i)}$  and an estimated variance  $\hat{\sigma}_{boot}^{2(i)}$ , a new approximated null distribution can be construed and the corresponding 95% sample quantile  $Q_{boot}^{(i)}(0.95)$  can be computed. Then, if  $\hat{D}_{boot}^{(i)} \geq Q_{boot}^{(i)}(0.95)$ ,  $H_0$  will be rejected for  $M_{boot}^{(i)}$ . The ratio of rejected  $M_{boot}^{(i)}$  among all the refitted models provides an indication of how often the assumed regression model are considered to be incorrect if the data can be obtained repetitively from the same data generating process. But this approach is computationally very expensive because it requires  $n_{boot} \times n_{null}$  times of residual plot assessment. In practice,



$Q_{null}(0.95)$  will be used to replace  $Q_{boot}^{(i)}(0.95)$  in the computation.

## 2.4. Generation of training data

### 2.4.1. Data generating process

While observational data is frequently employed in training models for real-world applications, the data generating process of observational data often remains unknown, making computation for our target variable  $D$  unattainable. Consequently, the computer vision models developed in this study were trained using synthetic data. This approach provides us with precise label annotations. Additionally, it ensures a large and diverse training dataset, as we have control over the data generating process, and the simulation of the training data is relatively cost-effective.

We have incorporated three types of residual departures of linear regression model in the training data, including non-linearity, heteroskedasticity and non-normality. All three departures can be summarised by the data generating process formulated as

$$\mathbf{y} = \mathbf{1}_n + \mathbf{x}_1 + \beta_1 \mathbf{x}_2 + \beta_2 (\mathbf{z} + \beta_1 \mathbf{w}) + \mathbf{k} \odot \boldsymbol{\varepsilon}, \quad (7)$$

$$\mathbf{z} = \text{He}_j(g(\mathbf{x}_1, 2)), \quad (8)$$

$$\mathbf{w} = \text{He}_j(g(\mathbf{x}_2, 2)), \quad (9)$$

$$\mathbf{k} = \sqrt{\mathbf{1}_n + b(2 - |a|)(\mathbf{x}_1 + \beta_1 \mathbf{x}_2 - a\mathbf{1}_n)^2}, \quad (10)$$

where  $\mathbf{y}$ ,  $\mathbf{x}_1$ ,  $\mathbf{x}_2$ ,  $\mathbf{z}$ ,  $\mathbf{w}$ ,  $\mathbf{k}$  and  $\boldsymbol{\varepsilon}$  are vectors of size  $n$ ,  $\mathbf{1}_n$  is a vector of ones of size  $n$ ,  $\mathbf{x}_1$  and  $\mathbf{x}_2$  are two independent predictors,  $\text{He}_j(\cdot)$  is the  $j$ th-order probabilist's Hermite polynomials (Hermite 1864), the  $\sqrt{(\cdot)}$  and  $(\cdot)^2$  operators are element-wise operators,  $\odot$  is the Hadamard product, and  $g(\cdot, k)$  is a scaling function to enforce the support of the random vector to be  $[-k, k]^n$  defined as

$$g(\mathbf{x}, k) = 2k \cdot \frac{\mathbf{x} - x_{\min} \mathbf{1}_n}{x_{\max} - x_{\min}} - k \mathbf{1}_n, \text{ for } k > 0,$$

where  $x_{min} = \min_{i \in \{1, \dots, n\}} x_i$ ,  $x_{max} = \max_{i \in \{1, \dots, n\}} x_i$  and  $x_i$  is the  $i$ -th entry of  $\mathbf{x}$ .

The residuals and fitted values of the fitted model is obtained by regressing  $\mathbf{y}$  on  $\mathbf{x}_1$ . This data generating process is adopted from Li et al. (2023) where it was used to simulate residual plots with non-linearity and heteroskedasticity visual patterns for human subject experiments.

In equation 7, predictor  $\mathbf{x}_1$  and  $\mathbf{x}_2$  are independent of each other, so excluding  $\mathbf{x}_2$  from the regression formula will not cause any problem. However,  $\mathbf{z}$  and  $\mathbf{w}$  are higher-order terms of  $\mathbf{x}_1$  and  $\mathbf{x}_2$ . If  $\beta_2 \neq 0$ , the regression model will suffer from non-linearity issues. Parameter  $j$  is a shape parameter controlling the number of tuning points of the non-linearity pattern. Generally, greater values of  $j$  will result in more tuning points.

Additionally, Scaling factor  $\mathbf{k}$  directly affects the error distribution and it is correlated with  $\mathbf{x}_1$  and  $\mathbf{x}_2$ . If  $b \neq 0$  and  $\varepsilon \sim N(\mathbf{0}_n, \sigma^2 \mathbf{I}_n)$ , the constant variance assumption will be violated. Parameter  $a$  is a shape parameter controlling the location of the smallest variance in a residual plot.

Non-normality violations are introduced by defining a non-normal distribution for  $\varepsilon$ .

- distribution of  $x_1$  and  $x_2$
- summary table of all the factor values
- example plots for the violations

#### 2.4.2. Computation of scagnostics

We have mentioned in Section 1 that scagnostics are a set of manually designed visual feature extraction functions. Although our computer vision model will learn its own feature extraction function during the training process, it will be beneficial to utilize additional information provided by scagnostics to help computer vision model making more accurate predictions.

For each generated residual plot, four scagnostics, namely, “Monotonic”, “Sparse”, “Splines” and “Striped” are computed using the `cassowary` R package (ref here). The computed measures along with the number of observations of the fitted model are provided as the second input of the computer vision model. Other scagnositcs are

also informative, but unfortunately, they are unavailable due to a fatal bug in the compiled C program of the `interp` R package (ref here) that will crash the process in a unpredictable manner. For reproducibility, we do not include these scagnostics in the training data.

#### 2.4.3. *Crafting a balanced training set*

In order to train a robust computer vision model, we intentionally control the distribution of the target variable  $D$  of the training data. Making it uniform between 0 and 7. This is accomplished by preparing 50 buckets each only accepts training samples with  $D$  between  $[7(i-1)/49, 7i/49)$  for  $i < 50$ , where  $i$  is the index of the  $i$ -th bucket. For the 50-th bucket, any training samples with  $D \geq 7$  will be accepted. We have prepared 80000 training images, so each bucket can only contain  $80000 \div 50 = 1600$  training samples. The simulator will repeatedly sample parameter values from the parameter sample, generate residuals and fitted values using the data generating process, compute the distance, and check if the sample can be accepted by the corresponding bucket, until all the buckets are full.

### 2.5. *Architecture of the computer vision model*

The architecture of the computer vision model is adopted from a existing architecture called VGG16 that proven to be performant in image classification (Simonyan and Zisserman 2014). The first layer is the input layer with shape  $n \times h \times w \times 3$  which could accept  $n$  RGB images, followed by a grayscale conversion layer using the luma formula under the CCIR 601 standard (ref here) to convert the colour image to an grey scale image. Grayscale is enough for our task since data points are plotted in black. Three different combinations of  $h$  and  $w$  are chosen to seek a sufficient large image resolution for this problem. This includes  $32 \times 32$ ,  $64 \times 64$  and  $128 \times 128$ .

The processed image is then used as the input of the first convolutional block. The model has at most five consecutive convolutional blocks which is similar to the original VGG16 architecture. In each block, there are two 2D convolutional layers followed by two activation layers respectively, and there is a 2D max pooling layer follows the

second activation layer. The 2D convolutional layer convolves the input with a fixed number of  $3 \times 3$  convolution filters, and the 2D max pooling layer downsamples the input along its spatial dimensions by taking the maximum value over a  $2 \times 2$  window for each channel of the input. The activation layer is set to be the rectified linear unit activation function (ReLU), which is a standard practice in deep learning. This introduces a non-linear transformation of the output of the 2D convolutional layer. Furthermore, to regularize the training, a batch normalization layer is added after each of the 2D convolutional layer and before the activation layer. A dropout layer is also appended at the end of each convolutional block to randomly set some inputs to zeros during training.

The output of the last convolutional block will be summarised by a global max pooling layer or a global average pooling layer to gain a two-dimensional tensor. Since we want to utilize the information contained in scagnostics, the two-dimensional tensor is concatenated with an additional  $n \times 5$  tensor, which contains the “Monotonic”, “Sparse”, “Splines” and “Striped” measures and the number of observations for  $n$  residual plots.

The concatenated tensor will be fed into the final prediction block. This block contains two fully-connected layers, the first one has at least 128 units followed by a dropout layer. Sometimes, a batch normalization layer will be inserted between the fully-connected layer and the dropout layer. The second fully-connected layer has only one unit, serves as the output of the model.

The model weights are randomly initialized and they are optimized by the Adam optimizer with the mean square error loss function. Therefore, we try to find a set of weights  $\hat{\theta}$  by

$$\hat{\theta} = \underset{\theta}{\operatorname{argmin}} \frac{1}{n_{train}} \sum_{i=1}^{n_{train}} (D_i - f_{\theta}(V_i, S_i))^2,$$

where  $n_{train}$  is the number of training samples,  $V_i$  is the  $i$ -th residual plot and  $S_i$  is the additional information about the  $i$ -th residual plot including four scagnostics and the number of observations.

- a diagram for the model

## 2.6. *Training and hyperparameter tuning*

To obtain an optimal deep learning model, hyperparameters such as learning rate often needs to be tuned via a tuner. In this study, we used the Bayesian optimization tuner from the `keras-tuner` Python library (ref here) to tune the hyperparameters. The complete list of hyperparameters is provided in Table 1.

The number of base filters determines the number of filters for the first 2D convolutional layer. In VGG16, the number of filters for the 2D convolutional layer in a block is 2 times the number in the previous block, except for the last block which has the same number of convolution filters as the previous one. This hyperparameter helps to control the complexity of the computer vision model. More base filters will result in more trainable parameters.

Similarly, the number of units for the first fully-connected layer determines the complexity of the final prediction block. And more units will lead to more trainable parameters.

Dropout rate and batch normalization are flexible hyperparameters which works jointly with other hyperparameters to smooth the training process. A high dropout rate is needed when the model learns too much noise from the training dataset. And a low dropout rate is needed when the model is complex and difficult to converge. Batch normalization on the other hand may be needed for solving the internal covariate shift problem due to randomness in the weight initialization and randomness in the input data.

Having additional inputs including the scagnostics and the number of observations could be beneficial for making more accurate prediction. So we let the tuner to decide if these inputs are actually needed.

Learning rate is one of the most important hyperparameters, and it determines the step size of the optimization algorithm. A high learning rate could help the model to avoid getting stuck in a local minimum, but it could also ruin the optimization process by jumping over the global minimum. A low learning rate could smooth the training process but it increases the time to converge and the chance of getting stuck in local

**Table 1.** Name of hyperparameters and their corresponding domain for the computer vision model.

Hyperparameter	Domain
Number of base filters	{4, 8, 16, 32, 64}
Dropout rate for convolutional blocks	[0.1, 0.6]
Batch normalization for convolutional blocks	{false, true}
Type of global pooling	{max, average}
Ignore additional inputs	{false, true}
Number of units for the fully-connected layer	{128, 256, 512, 1024, 2048}
Batch normalization for the fully-connected layer	{false, true}
Dropout rate for the fully-connected layer	[0.1, 0.6]
Learning rate	[1e-8, 1e-1]

minimum.

The model is trained on the M3 high-performance computing platform (ref here) with TensorFlow (ref here) and Keras (ref here). During the training process, 80% of the training data are used as the actual training data, and 20% of the training data are reserved as validation data. We let the Bayesian optimization tuner runs 100 trials to find the best hyperparameter values according to the validation root mean square error. The tuner will restore the best epoch of the best model from the trials. Early stopping is also applied such that the training process will halt if the validation root mean square error does not improve for 50 epochs. The maximum allowed epochs is 2000 where no models reach.

## 2.7. *Model evaluation methods*

- RMSE for the test set
- $R^2$
- Mean bias deviation to understand the overall bias
- quantile loss to understand how well the model captures the entire distribution of D
- Percentage of predictions within a tolerance interval (like 0.1)
- comparison with human visual inference
- overview of the human subject experiment
- metrics

**Table 2.** Hyperparameters values for the optimized computer vision models with different input sizes.

Hyperparameter	$32 \times 32$	$64 \times 64$	$128 \times 128$
Number of base filters	32	64	64
Dropout rate for convolutional blocks	0.4	0.3	0.4
Batch normalization for convolutional blocks	true	true	true
Type of global pooling	max	average	average
Ignore additional inputs	false	false	false
Number of units for the fully-connected layer	256	256	256
Batch normalization for the fully-connected layer	false	true	true
Dropout rate for the fully-connected layer	0.2	0.4	0.1
Learning rate	0.0003	0.0006	0.0052

- agreement rate
- check cases that are agreed
- check cases that are disagreed

### 3. Results

#### 3.1. *Optimized hyperparameters*

Based on the tuning process described in Section 2.6, the optimized hyperparameter values are provided in Table 2. It can be observed that at least 32 base filters are needed, and the preferable choice for the  $64 \times 64$  model and the  $128 \times 128$  model is 64 base filters, which is the same as the original VGG16 architecture. The optimized values for dropout rate for convolutional blocks is around 0.4. And applying batch normalization for convolutional blocks has a positive impact on the performance. All optimized models choose to preserve the additional inputs to reduce the validation error. The number of units needed for the fully-connected layer is 256, which is not a very large number comparing to the VGG16 classifier, suggesting that the problem we are trying to solve is relatively easy. The optimized learning rates are usually smaller than the default value recommended by Keras which is 0.001.

**Table 3.** The training and test performance of three optimized models with different input sizes.

	RMSE	$R^2$	MAE	Huber loss
<b>Training set</b>				
$32 \times 32$	0.531	0.937	0.364	0.126
$64 \times 64$	0.405	0.963	0.260	0.072
$128 \times 128$	0.432	0.959	0.290	0.084
<b>Test set</b>				
$32 \times 32$	0.660	0.901	0.434	0.181
$64 \times 64$	0.674	0.897	0.438	0.186
$128 \times 128$	0.692	0.892	0.460	0.199

### 3.2. Model performance

The training and test performance of optimized models with three different input sizes are provided in Table 3. Among these models, the  $64 \times 64$  model and the  $32 \times 32$  model are consistently having the best training and test performance respectively. The mean absolute error shows that the difference between  $\hat{D}$  and  $D$  is around 0.43 on the test set, which is very small considering the range of  $D$  is normally between 0 and 7. The high  $R^2$  also suggests the prediction is mostly linearly correlated with the target.

Figure 2 displays a hexagonal heatmap for  $D - \hat{D}$  vs  $D$ . For residual plots with  $D$  close to zero, all the optimized models tends to over-predict  $\hat{D}$ , leading to negative residuals. When  $D$  is between 1.5 and 6, the smooth curves indicate that  $\hat{D}$  is not heavily biased, and there are some instances where  $\hat{D}$  is severely under-predicted. And when  $D$  is greater than 6, there are more instances being under-predicted than over-predicted.

Given the model performance metrics, only the best model evaluated on the test set, i.e. the  $32 \times 32$  model, will be used in the following analysis.

### 3.3. Comparison with human visual inference

#### 3.3.1. Overview of the human subject experiment

In order to check the validity of the proposed computer vision model, residual plots presented in the human subject experiment conducted by Li et al. (2023) will be



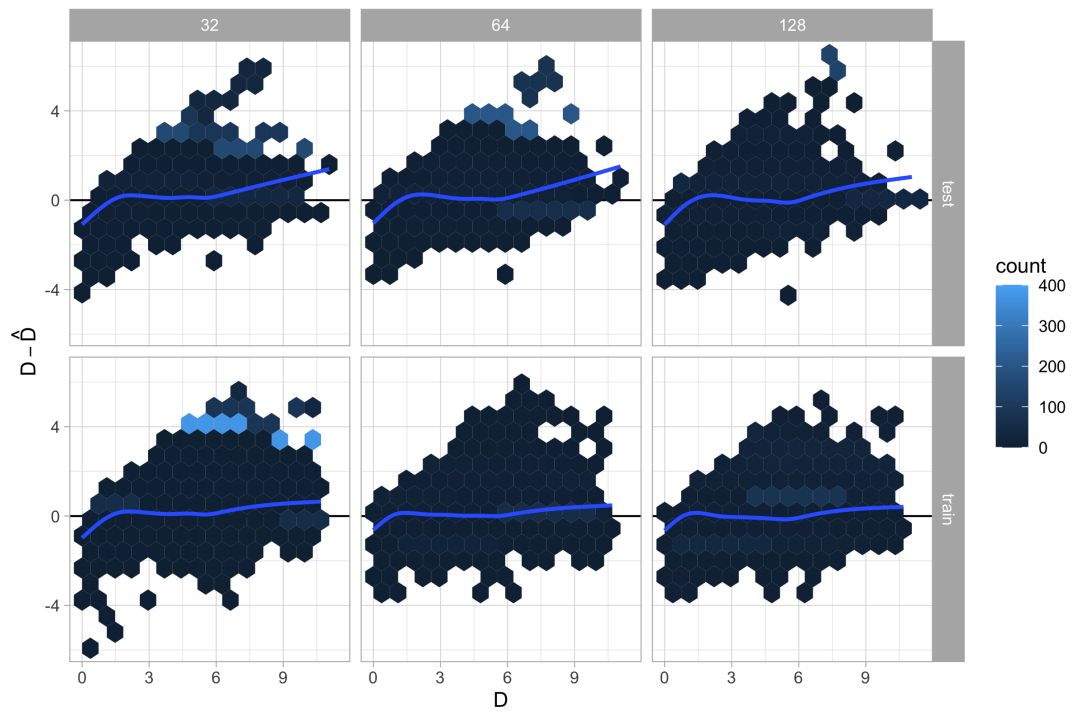


**Figure 2.** Hexagonal heatmap for residuals vs distance on training and test data for three optimized models with different input sizes. The blue lines are smoothing curves produced by fitting gnealized additive models.

assessed. This study has collected 7974 human responses to 1152 lineups. Each lineup contains one randomly placed actual residual plot and 19 null plots. Among the 1152 lineups, 24 are attention check lineups in which the visual patterns are designed to be extremely obvious and very different from the corresponding to null plots, 36 are null lineups where all the lineups consist of only null plots, 279 are lineups with uniform predictor distribution evaluated by 11 participants, and the remaining 813 are lineups with discrete, skewed or normal predictor distribution evaluated by 5 participants. Attention check lineups and null lineups will not be assessed in the following analysis.

In Li et al. (2023), the residual plots are simulated from a data generating process which is a special case of Equation 7. The main characteristic is the model violations are introduced separately, meaning non-linearity and heteroskedasticity will not co-exist in one lineup but assigned uniformly to all lineups. Additionally, non-normality and multiple predictors are not considered in their experimental design.

### 3.3.2. *Model performance on the human data*

For each lineup used in Li et al. (2023), there are one actual residual plot and 19 null plots. While the distance  $D$  for the actual residual plot depends on the underlying data generating process, the distance  $D$  for the null plots are zeros. We have used our optimized computer vision model to predict  $\hat{D}$  for both the actual residual plots and the null plots.

The performance metrics of  $\hat{D}$  for actual residual plots are provided in Table 4. It can be observed that all the performance metrics are slightly worse than the metrics evaluated on the test data. Still, the mean absolute error remains at a low level, and the linearly correlation between the prediction and the true value is still very high. Lineups with non-linearity issues are more difficult to be predicted than those with heteroskedasticity issues.

Figure 3 displays the  $D - \hat{D}$  vs  $D$  plot for actual residual plots used in the experiment. The behaviour of the prediction is roughly the same as what we can be observed from the evaluation of the test data. The model over-predicts  $\hat{D}$  when  $D$  is close to zero, and under-predicts  $\hat{D}$  when  $D$  is greater than 6. However, for residual plots with non-linearity issues, we do not observe the over-prediction for  $D > 6$  because there are

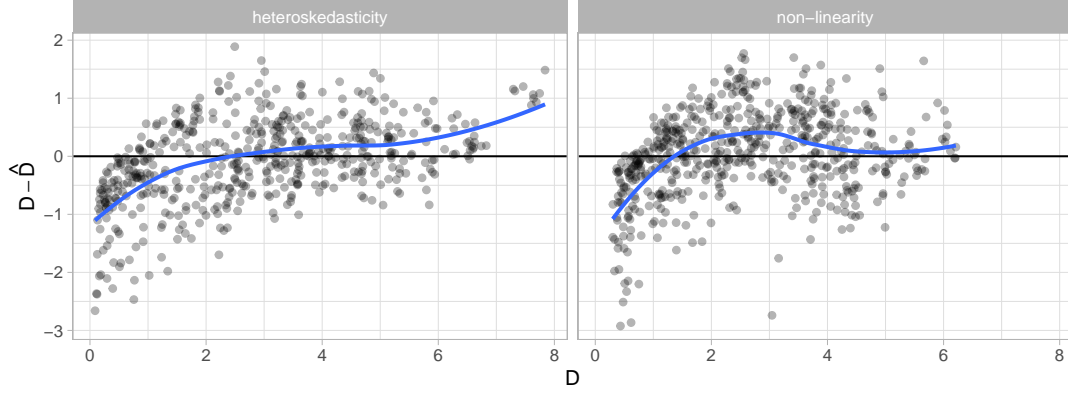


**Figure 3.** Residuals vs distance plot on lineups used in the human subject experiment. The blue line is a smoothing curve produced by fitting a generalized additive model.

**Table 4.** The performance of the  $32 \times 32$  model on the data used in the human subject experiment.

Voilation	RMSE	$R^2$	MAE	Huber loss
heteroskedasticity	0.721	0.852	0.553	0.235
non-linearity	0.738	0.770	0.566	0.246

not many cases in that area. And the over-prediction happens at around  $2 < D < 4$ .

For null plots, a histogram of the prediction is provided in Figure 4. In most cases,  $\hat{D}$  will be predicted at around 1. And as  $\hat{D}$  increases, the number of predictions decreases. There are some outliers with  $\hat{D} > 5$ .

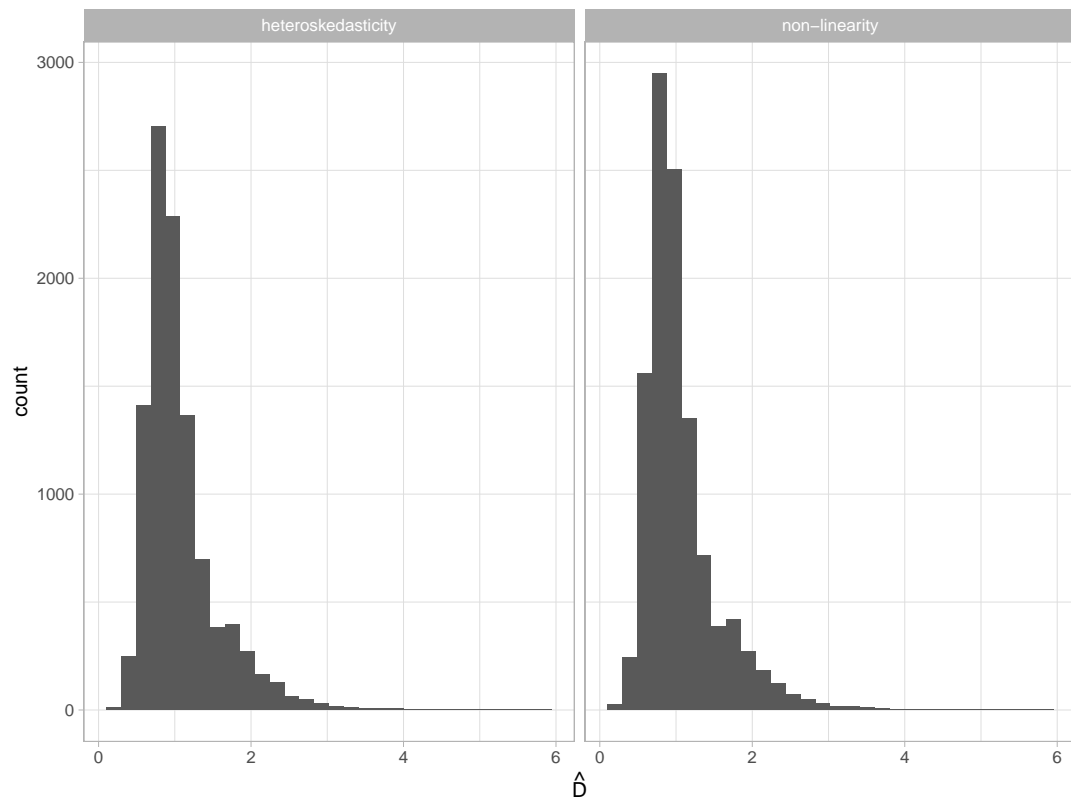
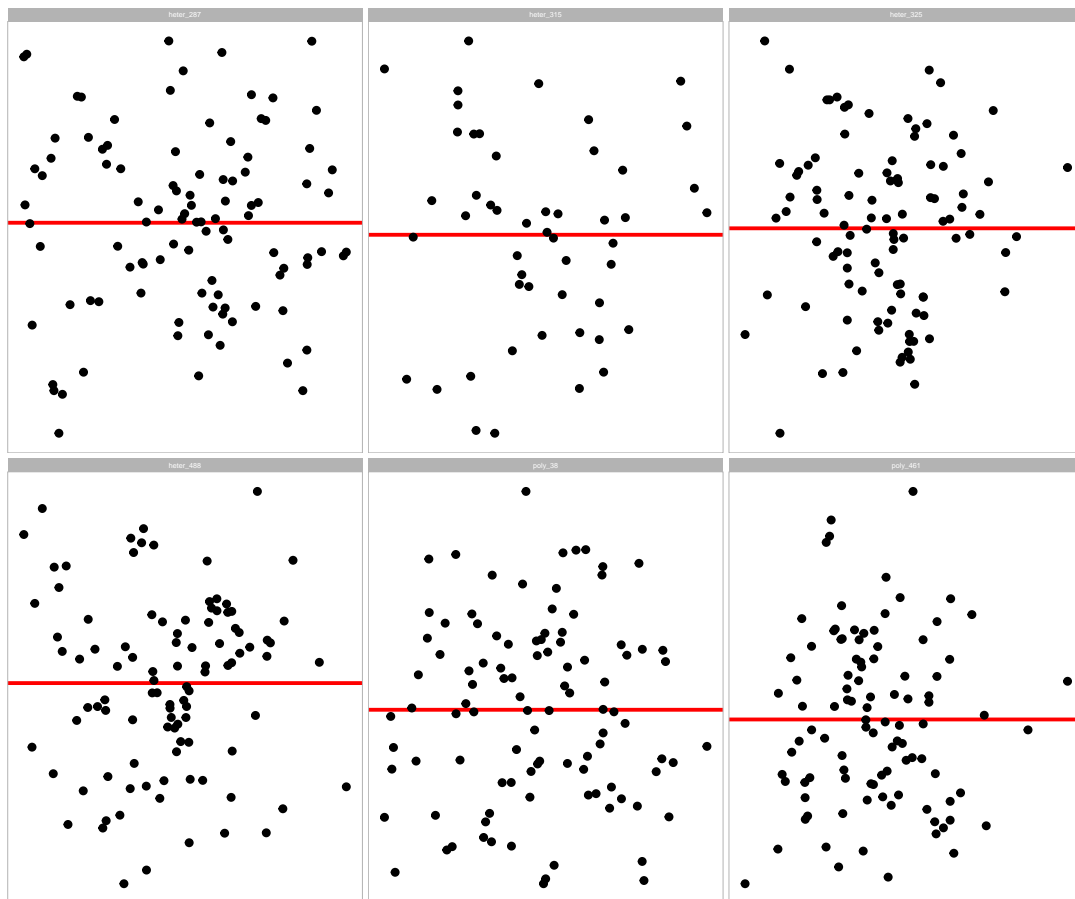


**Figure 4.** Histogram of predicted distance on null plots used in the human subject experiment.



### 3.4. *When the model works*

- simple examples (non-linearity, heteroskedasticity, ...)
- datasaurus

### 3.5. *When the model does not work*

- human detect but model does not
- cartoon residuals?

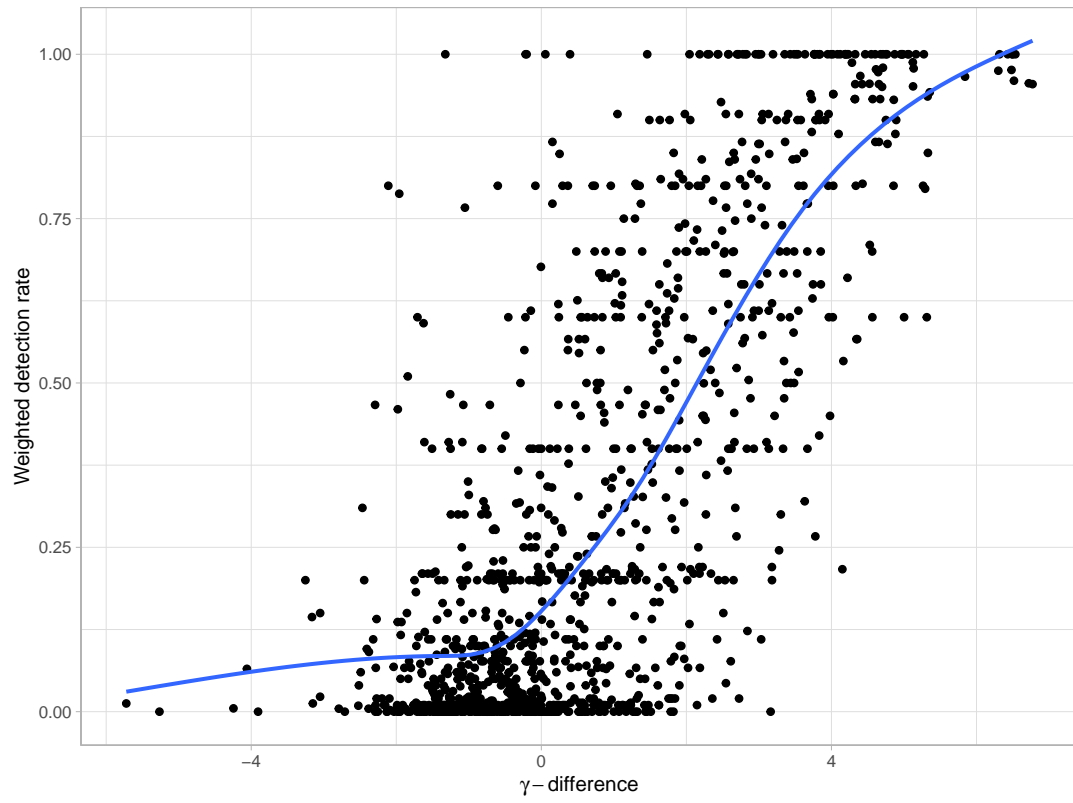


**Figure 5.** A weighted detection rate vs  $\delta$ -difference plot.

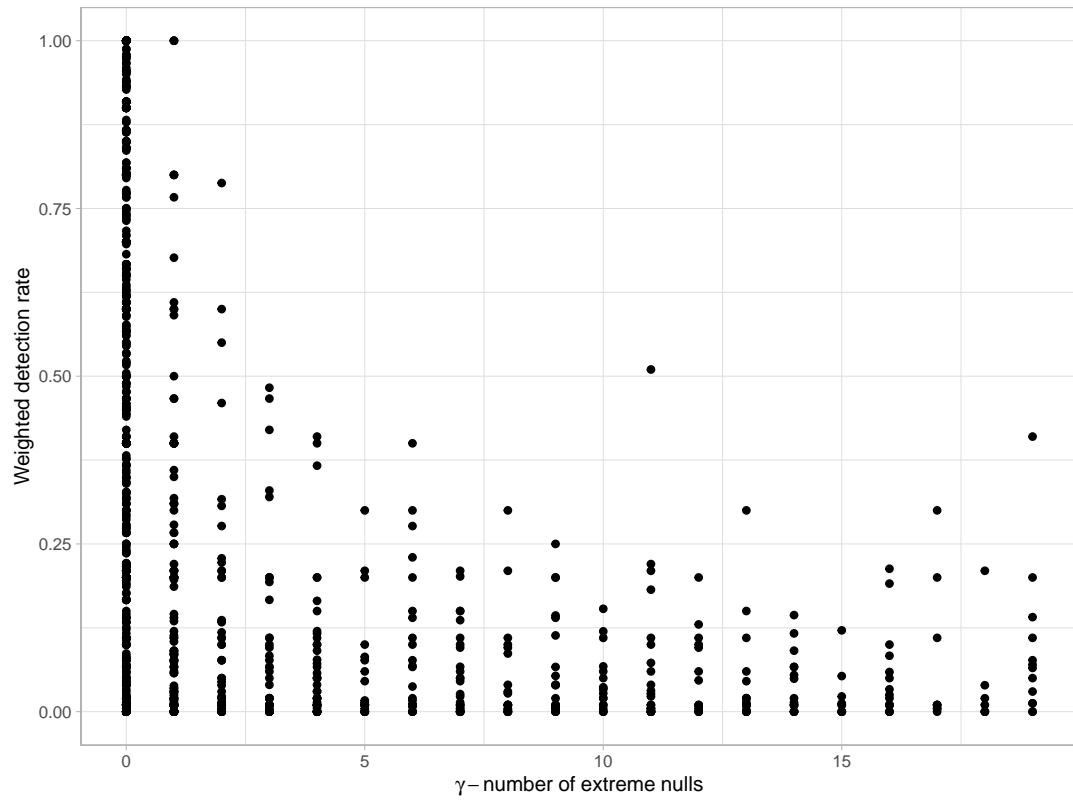


**Figure 6.** A weighted detection rate vs  $\gamma$ -number of extreme nulls plot.

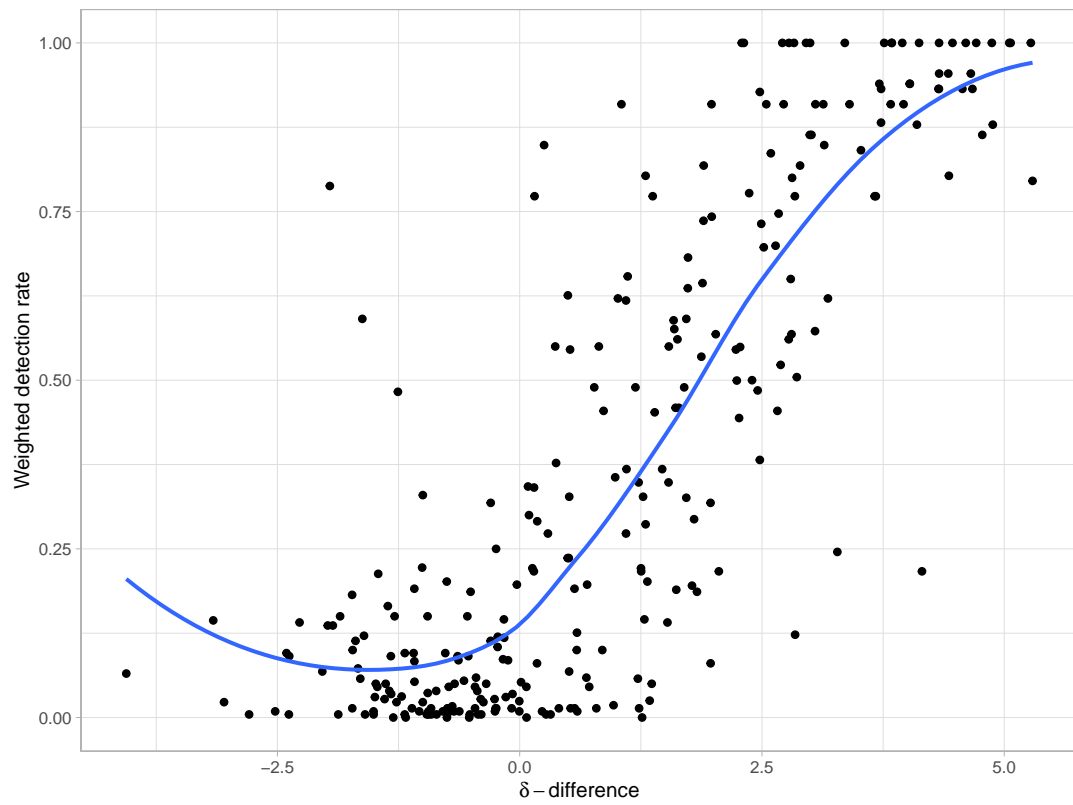


**Figure 7.** A weighted detection rate vs  $\delta$ -difference plot for lineups evaluated by 11 people.



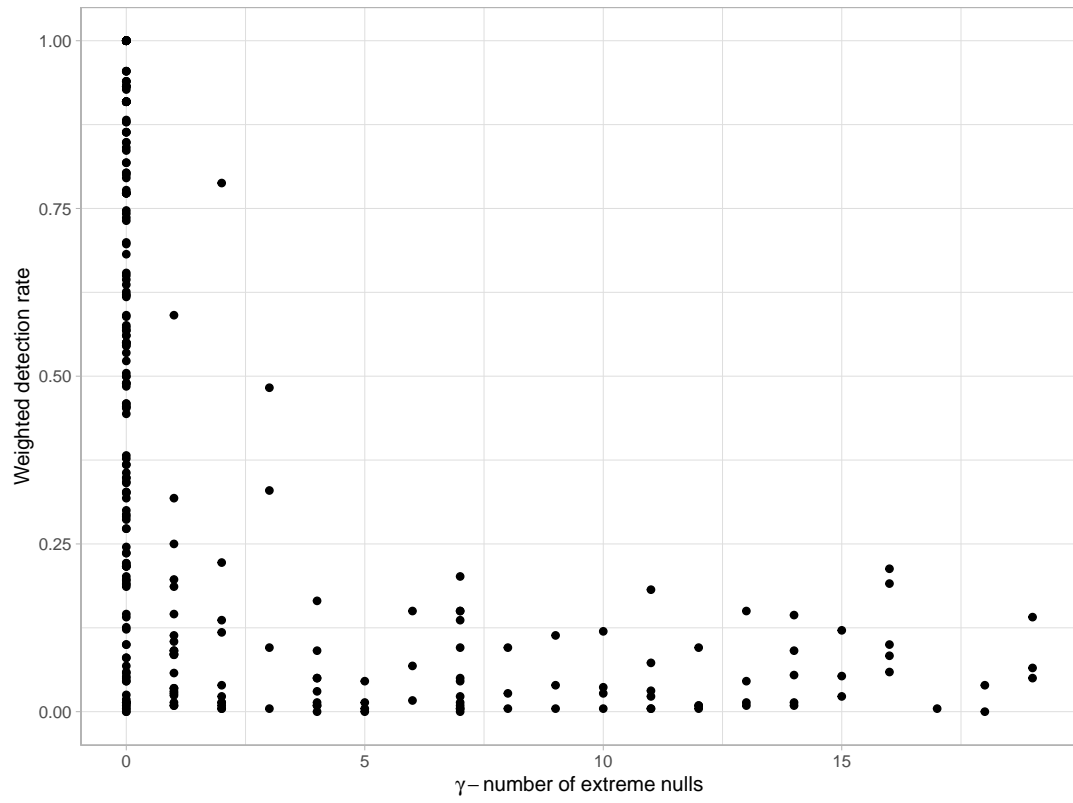


**Figure 8.** A weighted detection rate vs  $\gamma$ -number of extreme nulls plot for lineups evaluated by 11 people.

### 3.6. Workflow: how one use this model? (small showcase)

## 4. Discussion

There are other kinds of residual departures like autocorrelation that are not considered in this study. The primary goal of this paper is to establish a new way of evaluating residual plot and conducting visual test with computer vision models. Building computer vision models for other model violations and other types of diagnostic plots could be future directions of this field.

## 5. Conclusion

- Summary of findings
- Contributions to the field
- Future directions for research

## References

- Abadi, Martín, Ashish Agarwal, Paul Barham, Eugene Brevdo, Zhifeng Chen, Craig Citro, Greg S Corrado, et al. 2016. “Tensorflow: Large-scale machine learning on heterogeneous distributed systems.” *arXiv preprint arXiv:1603.04467* .
- Belsley, David A, Edwin Kuh, and Roy E Welsch. 1980. *Regression diagnostics: Identifying influential data and sources of collinearity*. John Wiley & Sons.
- Brunetti, Antonio, Domenico Buongiorno, Gianpaolo Francesco Trotta, and Vitoantonio Bevilacqua. 2018. “Computer vision and deep learning techniques for pedestrian detection and tracking: A survey.” *Neurocomputing* 300: 17–33.
- Buja, Andreas, Dianne Cook, Heike Hofmann, Michael Lawrence, Eun-Kyung Lee, Deborah F Swayne, and Hadley Wickham. 2009. “Statistical inference for exploratory data analysis and model diagnostics.” *Philosophical Transactions of the Royal Society A: Mathematical, Physical and Engineering Sciences* 367 (1906): 4361–4383.
- Chen, Yun, Shijie Su, and Hui Yang. 2020. “Convolutional neural network analysis of recurrence plots for anomaly detection.” *International Journal of Bifurcation and Chaos* 30 (01): 2050002.
- Chopra, Sumit, Raia Hadsell, and Yann LeCun. 2005. “Learning a similarity metric discrim-

- inatively, with application to face verification.” In *2005 IEEE computer society conference on computer vision and pattern recognition (CVPR’05)*, Vol. 1, 539–546. IEEE.
- Chowdhury, Niladri Roy, Dianne Cook, Heike Hofmann, and Mahbubul Majumder. 2018. “Measuring lineup difficulty by matching distance metrics with subject choices in crowd-sourced data.” *Journal of Computational and Graphical Statistics* 27 (1): 132–145.
- Chu, Hongyang, Xinwei Liao, Peng Dong, Zhiming Chen, Xiaoliang Zhao, and Jiandong Zou. 2019. “An automatic classification method of well testing plot based on convolutional neural network (CNN).” *Energies* 12 (15): 2846.
- Cook, R Dennis, and Sanford Weisberg. 1982. *Residuals and influence in regression*. New York: Chapman and Hall.
- Emami, Shervin, and Valentin Petrut Suci. 2012. “Facial recognition using OpenCV.” *Journal of Mobile, Embedded and Distributed Systems* 4 (1): 38–43.
- Frisch, Ragnar, and Frederick V Waugh. 1933. “Partial time regressions as compared with individual trends.” *Econometrica: Journal of the Econometric Society* 387–401.
- Fukushima, Kunihiro, and Sei Miyake. 1982. “Neocognitron: A new algorithm for pattern recognition tolerant of deformations and shifts in position.” *Pattern recognition* 15 (6): 455–469.
- Hailesilassie, Tameru. 2019. “Financial Market Prediction Using Recurrence Plot and Convolutional Neural Network.” .
- Hatami, Nima, Yann Gavet, and Johan Debayle. 2018. “Classification of time-series images using deep convolutional neural networks.” In *Tenth international conference on machine vision (ICMV 2017)*, Vol. 10696, 242–249. SPIE.
- Hermite, M. 1864. *Sur un nouveau développement en série des fonctions*. Imprimerie de Gauthier-Villars.
- Hyndman, Rob J, and Yanan Fan. 1996. “Sample quantiles in statistical packages.” *The American Statistician* 50 (4): 361–365.
- Krishnan, Ganesh, and Heike Hofmann. 2021. “Hierarchical Decision Ensembles-An inferential framework for uncertain Human-AI collaboration in forensic examinations.” *arXiv preprint arXiv:2111.01131* .
- Kullback, Solomon, and Richard A Leibler. 1951. “On information and sufficiency.” *The Annals of Mathematical Statistics* 22 (1): 79–86.
- Lee, Howard, and Yi-Ping Phoebe Chen. 2015. “Image based computer aided diagnosis system for cancer detection.” *Expert Systems with Applications* 42 (12): 5356–5365.

- Li, Weihao, Dianne Cook, Emi Tanaka, and Susan VanderPlas. 2023. “A Plot is Worth a Thousand Tests: Assessing Residual Diagnostics with the Lineup Protocol.” *arXiv preprint arXiv:2308.05964* .
- Loy, Adam, and Heike Hofmann. 2013. “Diagnostic tools for hierarchical linear models.” *Wiley Interdisciplinary Reviews: Computational Statistics* 5 (1): 48–61.
- Loy, Adam, and Heike Hofmann. 2014. “HLMdiag: A suite of diagnostics for hierarchical linear models in R.” *Journal of Statistical Software* 56: 1–28.
- Loy, Adam, and Heike Hofmann. 2015. “Are you normal? The problem of confounded residual structures in hierarchical linear models.” *Journal of Computational and Graphical Statistics* 24 (4): 1191–1209.
- Ojeda, Sun Arthur A, Geoffrey A Solano, and Elmer C Peramo. 2020. “Multivariate time series imaging for short-term precipitation forecasting using convolutional neural networks.” In *2020 International Conference on Artificial Intelligence in Information and Communication (ICAIIIC)*, 33–38. IEEE.
- Rawat, Waseem, and Zenghui Wang. 2017. “Deep convolutional neural networks for image classification: A comprehensive review.” *Neural computation* 29 (9): 2352–2449.
- Silverman, Bernard W. 2018. *Density estimation for statistics and data analysis*. Routledge.
- Simonyan, Karen, and Andrew Zisserman. 2014. “Very deep convolutional networks for large-scale image recognition.” *arXiv preprint arXiv:1409.1556* .
- Singh, Karamjit, Garima Gupta, Lovekesh Vig, Gautam Shroff, and Puneet Agarwal. 2017. “Deep convolutional neural networks for pairwise causality.” *arXiv preprint arXiv:1701.00597* .
- Tukey, John W, and Paul A Tukey. 1985. “Computer graphics and exploratory data analysis: An introduction.” In *Proceedings of the sixth annual conference and exposition: computer graphics*, Vol. 85, 773–785.
- Wang, Zhou, Alan C Bovik, Hamid R Sheikh, and Eero P Simoncelli. 2004. “Image quality assessment: from error visibility to structural similarity.” *IEEE transactions on image processing* 13 (4): 600–612.
- Widen, Holly M, James B Elsner, Stephanie Pau, and Christopher K Uejio. 2016. “Graphical inference in geographical research.” *Geographical Analysis* 48 (2): 115–131.
- Wilkinson, Leland, Anushka Anand, and Robert Grossman. 2005. “Graph-theoretic scagnostics.” In *Information Visualization, IEEE Symposium on*, 21–21. IEEE Computer Society.
- Zhang, Ye, Yi Hou, Shilin Zhou, and Kewei Ouyang. 2020. “Encoding time series as multi-

scale signed recurrence plots for classification using fully convolutional networks.” *Sensors* 20 (14): 3818.